

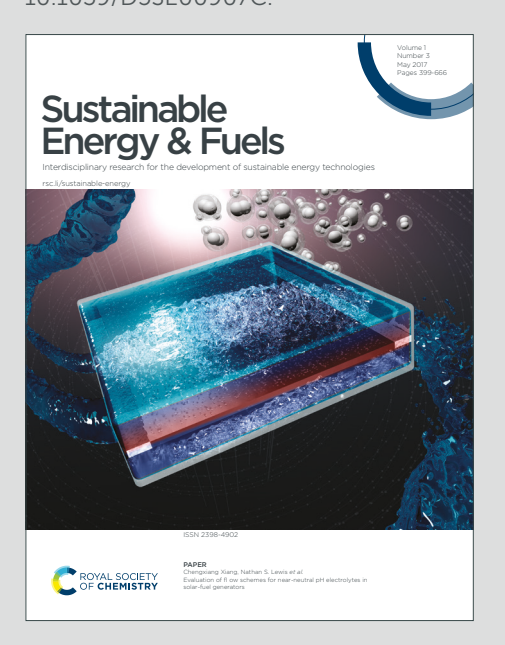
# Sustainable Energy & Fuels



Interdisciplinary research for the development of sustainable energy technologies

Accepted Manuscript

This article can be cited before page numbers have been issued, to do this please use: P. P. Machado Pico, J. Montero, A. Tsurumaki, S. Passerini and M. A. Navarra, *Sustainable Energy Fuels*, 2025, DOI: 10.1039/D5SE00907C.



This is an Accepted Manuscript, which has been through the Royal Society of Chemistry peer review process and has been accepted for publication.

Accepted Manuscripts are published online shortly after acceptance, before technical editing, formatting and proof reading. Using this free service, authors can make their results available to the community, in citable form, before we publish the edited article. We will replace this Accepted Manuscript with the edited and formatted Advance Article as soon as it is available.

You can find more information about Accepted Manuscripts in the <u>Information for Authors</u>.

Please note that technical editing may introduce minor changes to the text and/or graphics, which may alter content. The journal's standard <u>Terms & Conditions</u> and the <u>Ethical guidelines</u> still apply. In no event shall the Royal Society of Chemistry be held responsible for any errors or omissions in this Accepted Manuscript or any consequences arising from the use of any information it contains.



This article is licensed under a Creative Commons Attribution-NonCommercial 3.0 Unported Licence Open Access Article. Published on 28

2025. Downloaded on 23/11/25 21:19:17.

View Article Online DOI: 10.1039/D5SE00907C

# **ARTICLE**

# Bifunctional PGM-free electrocatalysts for seawater batteries

Pedro Pablo Machado Pico<sup>a</sup>, Jorge Montero<sup>a</sup>, Akiko Tsurumaki\*<sup>a,d</sup>, Stefano Passerini<sup>b,c</sup>, Maria Assunta Navarra\*a,d

Received 00th January 20xx. Accepted 00th January 20xx

DOI: 10.1039/x0xx00000x

Seawater batteries (SWBs) are an emerging energy storage solution that leverages the abundant and cost-effective sodium ions present in seawater. However, their performance is often constrained by the sluggish kinetics of the oxygen evolution reaction (OER) and oxygen reduction reaction (ORR) at the seawater cathode. To overcome these limitations, a series of platinum group metal (PGM)-free bifunctional electrocatalysts was developed to enhance OER/ORR catalytic activity and overall power performance. Metal-doped nitrogen carbon nanoparticles (M-N-C), namely FeNiNC, FeNC, and NiNC, were synthesized via a simple precipitation method followed by heat treatment, yielding an amorphous structure that promotes improved capacitive behavior. The use of low-cost biomass derived from hazelnut shells as a carbon-based material, modified with Fe and/or Ni, resulted in a highly efficient catalyst. Particularly, FeNiNC exhibited an ORR activity of 0.87 V vs. RHE at half-potential and an OER activity of 1.57 V vs. RHE at a current density of 10 mA cm<sup>-2</sup>. Electrochemical characterization demonstrated that SWBs incorporating the FeNiNC catalyst achieved significantly enhanced power output and cycling stability, maintaining performance for 350 hours.

## Introduction

Rechargeable seawater batteries (SWBs) are innovative and promising sustainable energy storage devices, primarily due to the abundance and renewability of their cathode material, i.e., seawater. The system operates utilizing hydroxide OH- ions present in seawater with the Na<sup>+</sup> ions present in the anodic compartment. During charging, sodium ions gain electrons from the cathode, where O₂ is formed through the oxygen evolution reaction (OER). Conversely, during discharge, dissolved O₂ in water is reduced back to OH- via the oxygen reduction reaction (ORR)[1]. Theoretically, OER and ORR occur at approximately 3.4 V vs Na/Na<sup>+</sup> in nearly pH-neutral seawater (pH ≈ 8) [2]. While this OER/ORR mechanism offers the advantage of seawater, being an abundant and renewable cathode material, the slow kinetics of these reactions result in significant overpotentials during operation. In typical seawater battery setups, where carbon paper is immersed in seawater, the potential plateaus for OER and ORR appear at 3.9 V and 2.8 V vs Na/Na<sup>+</sup>, respectively [3]. This large overpotential highlights the need for efficient bifunctional electrocatalysts to enhance reaction kinetics [4].

The most commonly used catalysts for ORR and OER are based on platinum group metals (PGMs), such as Pt and IrO<sub>2</sub>/RuO<sub>2</sub> being the standard choices for these reactions, respectively. However, the limited availability and high cost of PGM catalysts pose significant barriers to the commercial viability of devices relying on these reactions, including SWBs [5]. The first PGM-free catalysts explored for SWBs were cobalt manganese oxides (CMOs), synthesized through the pyrolysis of a Prussian blue analogue, Mn₃[Co(CN)<sub>6</sub>]<sub>2</sub>·nH<sub>2</sub>O. The SWBs employing CMO demonstrated a relatively small voltage gap of approximately 0.53 V, which is notably lower than the gaps observed with commercial Pt/C ( $\sim$ 0.64 V) and Ir/C ( $\sim$ 0.73 V) catalysts and much smaller than that of SWBs without any catalyst ( $\sim$ 1.05 V) during the initial cycle [3].

The ORR at active sites can proceed via two main pathways: a two-electron transfer forming H<sub>2</sub>O<sub>2</sub>/HO<sub>2</sub><sup>-</sup> and a four-electron transfer producing H₂O/OH⁻. The latter pathway is preferred due to its faster kinetics [6,7]. Various families of PGM-free catalysts have been studied for ORR catalysis, including spinels [3,8], perovskites [9], and metal-organic frameworks [10]. For the OER, the performance is constrained by the formation of multiple intermediates, from  $OH^-$  to  $O_2$ . Optimizing OERcatalysts involves regulating the binding energies of these reactive intermediates, thereby improving the adsorption and desorption processes of OH- and O2 [11]. Several catalyst families, including metal alloys [12,13], phosphides [14], and chalcogenides [15], have been studied to enhance OER kinetics.

Among PGM-free materials, metal-nitrogen-carbon (M-N-C) catalysts are the most significant due to their high ORR activity and strong tolerance to contaminants [16]. These electrocatalysts contain diverse catalytic sites, including pyrrolic, pyridinic, and M-N<sub>x</sub> configurations [17], where the coordination of metal atoms to nitrogen atoms enhances the

<sup>&</sup>lt;sup>a.</sup> Department of Chemistry, Sapienza University of Rome, P.le A. Moro 5, 00185,

<sup>&</sup>lt;sup>b.</sup> KIT Campus Transfer GmbH, Haid-und-Neu-Str.7, 76131 Karlsruhe, Germany.

<sup>&</sup>lt;sup>c.</sup> Austrian Institute of Technology (AIT), Center for Transport Technologies, Giefinggasse 2, 1220 Vienna, Austria.

d. Hydro-Eco Research Center, Sapienza University of Rome, Via A. Scarpa 16, 00161. Rome. Italy.

<sup>†</sup> Footnotes relating to the title and/or authors should appear here. Supplementary Information available: [details of any supplementary information available should be included here]. See DOI: 10.1039/x0xx00000x

2025. Downloaded on 23/11/25 21:19:17.

**ARTICLE** Journal Name

direct four-electron reduction of oxygen to water [18,19]. Ndoping of carbon substrates is essential for stabilizing transition metal coordination, maintaining a high density of M-N<sub>x</sub> active sites, and preventing catalyst aggregation [20]. Among various metal precursors, iron(II) phthalocyanine has gained particular interest for the synthesis of Fe-N-C catalysts owing to its low cost, tunable electronic structure, facile synthesis, and low ORR overpotential [21,22]. Moreover, incorporating Fe with secondary metals such as Ni or Co is advantageous for OER catalysis, as the modification of the 3d orbital structure increases metal-O covalency [23]. In this bimetallic context, Fe-N<sub>x</sub> moieties act as dominant active sites for ORR by facilitating O<sub>2</sub> adsorption and accelerating the first electron transfer to form OOH\* intermediates, thereby reducing the energy barrier of the rate-determining step. In contrast, Ni centers contribute to OER by stabilizing high-valence Ni3+/Ni4+ species during anodic polarization, promoting both the formation and deprotonation of OOH\* intermediates. The close spatial proximity of Fe-N and Ni-N sites further enhance electron redistribution and optimizes intermediate binding energies, effectively lowering the energy barriers for OOH\* generation and decomposition in both reaction pathways [24-26].

To emphasize sustainable feature of SWBs, biomass-derived carbon materials are highly suitable due to their ecofriendliness, abundance, and renewability as well as other properties suitable for electrode applications such as high specific surface area, desirable electrical conductivity, tuneable porosity (micro, meso, and macro), and excellent thermal and chemical stability. Nitrogen-doped carbon derived from biomass improves electrical conductivity, enhances electrondonor properties, expands graphite layer spacing, increases the number of electroactive sites, and generates defect sites that provide ample space for electrolyte ions, thereby enhancing electrochemical reactivity and energy storage performance. Moreover, nitrogen self-doping has been reported to improve structural stability while tuning electronic properties and electrochemical activity [27,28]. In this context, a one-step pyrolysis treatment of biomass doped with a nitrogen source offers a simple, cost-effective, and eco-friendly approach for producing N-doped biochar. This method not only efficiently uses the carbon content of biomass, but also enhances its electrochemical properties for various energy storage and conversion applications [29-32].

In this work, we developed a synthesis strategy to prepare a FeNi-N-C bifunctional catalyst through wet impregnation followed by pyrolysis. The metal precursors consisted of iron(II) phthalocyanine and nickel(II) phthalocyanine, while urea served as both nitrogen and additional metal-coordination source. Functionalized biochar was employed as a conductive carbon support. Within this structure, Fe sites act as the primary active centers, whereas Ni sites modulate the local coordination environment, thereby optimizing the adsorption and desorption of oxygen intermediates [33]. The synthesized bifunctional FeNi-N-C catalyst was integrated into SWBs, showing desirable catalytic performance arises from the synergistic interplay between atomically dispersed Fe and Ni species coordinated to nitrogen within the carbon matrix.

# **Materials and Methods**

View Article Online DOI: 10.1039/D5SE00907C

#### Materials

Iron (II) phthalocyanine (FePc, Sigma-Aldrich), nickel (II) phthalocyanine (NiPc, Sigma), CH<sub>4</sub>N<sub>2</sub>O (urea, VWR Chemicals), ethanol (VWR Chemicals), isopropanol (Sigma-Aldrich), dimethylacetamide (DMA, Sigma-Aldrich), Nafion (5 wt.% in lower aliphatic alcohols and water, Ion Power), diethylene glycol dimethyl ether (DEGDME, Sigma-Aldrich), biphenyl (BP, Sigma-Aldrich), activated carbon cloth (Kynol), and Pt/C-RuO<sub>2</sub> (ElectroChem, Inc) were purchased and used without purification.

#### Carbon support and catalyst preparation

Synthesis of carbon support: Hazelnut shells were ball-milled in a Zirconia jar (V = 500 mL) with 100 Zirconia balls (10-mm diameter) in a planetary ball-miller (Pulverisette 6, Fritsch GmbH) for 6 h (45 min milled with 15 min pause) at a rotation rate of 400 rpm. Subsequently, 40 mg of the milled hazelnut powder and 160 mg of urea were mixed using a mortar and then pyrolyzed at different temperatures (700 or 900 °C) for 1 h under Ar atmosphere, yielding two samples labelled as NC7 and NC9 according to the temperature values.

Preparation of M-N-C catalysts: 100 mg of FePc and 100 mg of NiPc were mixed using a mortar for 10 min and then stirring overnight in 50 ml of DMA. The solution was dried at 80 °C to obtain a FeNi compound. The obtained FeNi powder (100 mg) and NC7 powder were mixed by hand using a mortar for 30 min, and then pyrolyzed in an Al<sub>2</sub>O<sub>3</sub>-tube furnace at 900 °C for 1 h under an Ar atmosphere, obtaining a sample labelled as FeNiNC. The FeNC and NiNC were prepared using the same preparations as FeNiNC by using either FePc or NiPc.

Catalyst ink preparation for RDE: The catalyst ink was prepared by dispersing 5 mg of the catalyst in 985  $\mu L$  of Milli-Q water and 15  $\mu$ L of isopropanol mixture. This dispersion was treated in an ultrasonic bath at 60 Hz for 45 min. Then, 15  $\mu$ L of Nafion solution was added to the dispersion, further treated in the ultrasonic bath for 15 min. The ink was dropped (10  $\mu$ L) onto a working electrode (glassy carbon disk electrode RDE, area = 0.247 cm<sup>2</sup>, Pine Research Instrumentation), resulting in a catalyst loading of 0.2 mg cm<sup>-2</sup>. Before use, the modified glassy carbon electrode was dried in a convection oven at 40 °C for 4 min.

# Seawater batteries configuration

Preparation of NaBP/DEGDME anolyte: DEGDME was dried over molecular sieves (4 Å, 8-12 mesh) for three days. Subsequently, BP was added into the dried DEGDME solvent to obtain a 1 M solution. The 1 M BP-DEGDME solution was stirred until complete dissolution, then Na metal was added to the solution to obtain a concentration of 1.1 M in sodium. After stirring for 2 h a dark blue solution of NaBP/DEGDME was obtained.

Cathode preparation: A total of 25 mg of FeNiNC was added to 2 mL of ethanol and stirred for 30 minutes. Then, 970 µL of Nafion (5 wt.% dispersion) were added to the solution, followed by continuous stirring for additional 30 minutes. The resulting ink was applied via spray coating to a 4 × 4 cm carbon cloth 2025. Downloaded on 23/11/25 21:19:17.

**ARTICLE** Journal Name

placed on a hot plate at 50 °C. Reference electrodes containing Pt/C-RuO<sub>2</sub> were prepared using the same procedure. In all cases, the final catalyst loading was 2 mg cm<sup>-2</sup>. This value was chosen because it provides a good balance between ensuring sufficient active sites for catalytic activity, maintaining favorable mass transfer, and avoiding underutilization of the inner catalyst layer [34].

SWBs assembly: 2465-type coin cells with a NASICON (Na<sub>3</sub>Zr<sub>2</sub>Si<sub>2</sub>PO<sub>12</sub>) window, supplied by 4 TO ONE, were assembled using a disc of Nickel foam that worked as anodic current collector, embedded with a NaBP/DEGDME solution as the anolyte in a glovebox. The sealed coin cells were immersed in artificial seawater comprising about 0.47 M NaCl. To the same seawater, a carbon cloth cathode coated with Pt/C-RuO2 or FeNiNC catalyst was immersed as the positive electrode. These set up were based on seawater flow cell testers supplied by 4 TO ONE.

#### Microstructural characterizations

The catalyst surface morphology was investigated using a Thermo Fisher Scientific Phenom ProX Desktop scanning electron microscopy and Energy dispersive spectroscopy (SEM-EDS) and High-resolution transmission electron microscopy (HR-TEM) JEOL F-200 assembled with a GATAN Rio16 CMOS acquisition camera and a JEOL EDX spectrometer. Brunauer-Emmett-Teller (BET) analysis was conducted using BELSORP MAX G from Microtrac to determine surface area and pore size

Raman spectroscopy was conducted using a Dilor Labram instrument equipped with a He-Ne laser source at 632.7 nm and a CCD cooled detector, which was calibrated with Si as the standard. The spectra were fitted using the Voigt function implemented in the Origin lab.

# **Electrochemical measurements**

Voltammetry: The catalytic activity toward ORR and OER of the prepared electrodes was examined by two steps: (1) cyclic voltammetry (CV) for both activation and evaluation and (2) linear sweep voltammetry (LSV) for evaluation, using a VMP Multichannel Potentiostat. A conventional three electrode cell was used. The reference electrode was Ag/AgCl (Amel 303/SCG/12), the auxiliary electrode was a graphite rod, and the glassy carbon rotating disk electrode (RDE) modified with the catalyst layer was a working electrode (see a former section for the preparation). CVs were carried out in either N2- or O2saturated aqueous 0.1 M KOH solution; prior to the measurements, the electrodes were activated by performing 100 and 50 CV cycles at 500 and 20 mV s<sup>-1</sup>, respectively.

To assess ORR and OER activity LSV-RDE experiments were carried out at a scan rate of 10 mV s<sup>-1</sup> and electrode rotation speed of 1600 rpm. The electrode potential was measured vs. Ag/AgCl and then converted to the reversible hydrogen electrode (RHE) scale, according to Equation (1):

$$E_{RHE} = E_{Ag/AgCI} + E^{0}_{Ag/AgCI} + 0.0591pH$$
 (1) where  $E^{0}_{Ag/AgCI} = 0.197 \text{ V}$ .

Galvanostatic charge-discharge: Cyclation of SWBs was carried out at a current density of 0.3 mA cm  $^{-2}\mbox{\rm Qut}^{-0}\mbox{\rm H}^{3}\mbox{\rm 2/RhAH})^{0}\mbox{\rm With}$ voltage limits of 4.0 V vs Na<sup>+</sup>/Na for charge and 2.5 V vs Na<sup>+</sup>/Na for discharge.

# Results and discussions

#### Materials Characterizations

The influence of thermal treatment temperature on hazelnut shell-derived carbon materials, namely, NC7 and NC9, as well as the effect of urea addition (C7) were also studied as summarized in the supplementary information (Figure S1a-f: SEM images and S1g: key elemental composition). Pore formation was not observed in the sample prepared without urea at 700 °C (Figure S1a,d). In contrast, when urea was added, distinct holes and cracks appeared on the surfaces of NC7 (Figure S1b,e) and NC9 (Figure S1c,f), confirming that urea addition promotes pore formation, as previously reported in the literature [35]. Elemental analysis was conducted using EDS spectroscopy as summarized in S1g, showing increase in C content and decrease in O and N contents at a higher temperature, i.e., 900 °C. Increasing the carbonization temperature generally promotes a higher degree of graphitization and enhances porosity [36]. However, this improvement occurs at the expense of nitrogen retention, as many nitrogen-containing functional groups like pyridinic and pyrrolic species, which are considered the most catalytically active, tend to decompose at elevated temperatures [37-40].

Enhanced porosity of NC7 and NC9, with respect to C7, was also confirmed by BET analysis. As shown in Figure S2, the N2 adsorption/desorption isotherms of all samples exhibit type I behavior, which is characteristic of microporous materials with pore sizes smaller than 2 nm [41, 42]. Quantitative analysis revealed that the specific surface area of the urea-undoped C7 was 46.96 m<sup>2</sup> g<sup>-1</sup>, while urea doping significantly increased the surface area to  $397.93 \text{ m}^2 \text{ g}^{-1}$  for NC7 and  $405.37 \text{ m}^2 \text{ g}^{-1}$  for NC9. Considering the similar porous structures of NC7 and NC9, together with a slightly higher proportion of catalytically active nitrogen functionalities and a lower energy requirement for NC7 synthesis, NC7 was selected as the nitrogen-carbon support for subsequent studies, offering advantages in both catalytic performance and sustainability.

Employing the selected NC7 (hereafter referred to as NC), the bifunctional catalyst FeNiNC was synthesized. The surface area further increased to 419.44 m<sup>2</sup> g<sup>-1</sup> for the FeNiNC composite, which is in good agreement with previous reports on FeNi–N–C electrocatalysts [43-45]. SEM-EDX mapping images of the FeNiNC samples, reported in Figure 1, confirmed the presence of C, N, O, K, Ni, and Fe in both the precursor and the final catalyst. The presence of K originates from the pristine hazelnut sample (see Table S2). Upon introducing Fe and Ni to form FeNiNC, the concentration of C and O increased, while those of N decreased, likely due to partial loss of N species at elevated temperatures. EDS mapping images of Fe and Ni (Figure 1) verify the uniform distribution of metal species across

Open Access Article. Published on 28 2025. Downloaded on 23/11/25 21:19:17.

This article is licensed under a Creative Commons Attribution-NonCommercial 3.0 Unported Licence.

ARTICLE Journal Name

the biochar surface, with no significant agglomeration observed.

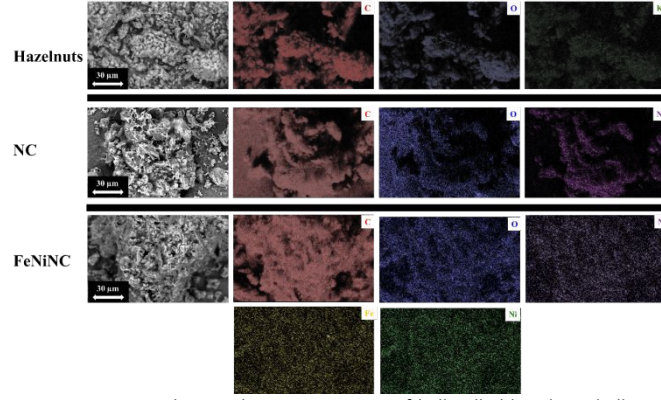


Figure 1. SEM-EDS elemental mapping images of ball-milled hazelnut shells, NC formed at 700  $^{\circ}\text{C}$  and final FeNiNC catalyst.

As shown in Figure 2a, the Raman spectra of the catalysts were collected to assess the degree of graphitization of the carbon substrate. Generally, the intensity ratio of the D to G bands ( $I_D/I_G$ ) serves as an indicator of graphitization. Among the various  $sp^2$ -hybridized forms of carbon, the D-band at  $1350~cm^{-1}$  corresponds to defects in the amorphous carbon structure, while the G-band at  $1580~cm^{-1}$  stands for the tangential vibration of  $sp^2$ -bonded carbon atoms. The intensity ratio between the D and G bands remained nearly identical for the FeNiNC catalyst and the monometallic catalysts, indicating that the introduction of metal did not significantly alter the graphitization degree of the carbon support, besides the increase in carbon content.

The crystal structure of catalysts was investigated by XRD measurement. As shown in Figure 2b, all three samples show the typical broad diffraction peak at 25.8° of the (002) lattice plane of graphitic carbon, indicating the occurrence of a partial graphitization. For the NiNC sample, the peaks at 44.5°, 51.8°, 76.3° can be assigned to Ni (JCPDS #04-0850) and those at 37.2°, 43.3°, and 75.4° to NiO (JCPDS #47-1049). The peaks associated with NiO are weaker than those of Ni, indicating that Ni is mostly present in its metallic form. In contrast, Fe is predominantly present in the oxidized form in FeNC as evidenced by the strong diffraction peaks at 30°, 35°, 43.5°, 53.9°, 57.5° and 63.1° corresponding to  $\gamma$ -Fe<sub>2</sub>O<sub>3</sub> (JCPDS #65-3107) along with a weak signal at 44.3° attributed to metallic Fe (JCPDS #06-0696). FeNiNC sample shows three distinct diffraction peaks at 44.1°, 51.4°, and 75.6° indexed to the (111), (200), and (220) crystal faces of FeNi alloy (JCPDS No. 38-0419) in addition to the minor features due to γ-Fe<sub>2</sub>O<sub>3</sub>.

In addition, HR-TEM and EDX analyses were performed to gain deeper insights into the FeNiNC sample (Figure S3). The HR-TEM images revealed the formation of FeNi nanocompounds with an average particle diameter of approximately 15 nm, a value consistent with previous reports [46]. Furthermore, EDX analysis indicated that the alloy is slightly Ni-rich, containing 38.27 wt% Fe and 61.73 wt% Ni, corresponding to an approximate atomic ratio of 1:1.5.

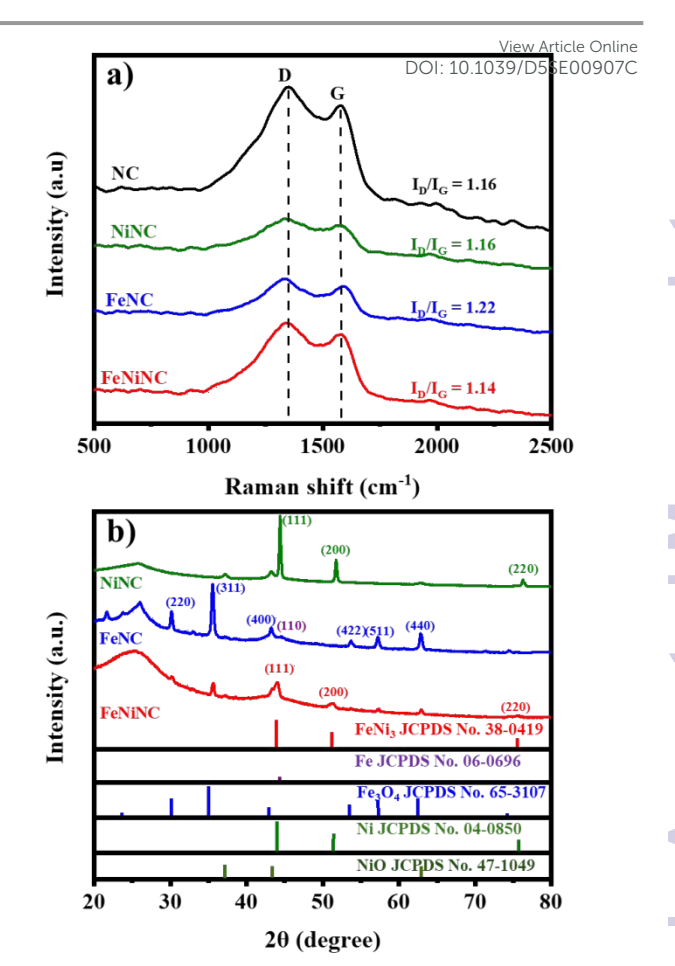


Figure 2. (a) Raman spectra of NC precursor formed at 700 °C, and FeNC, NiNC and FeNiNC catalysts; (b) XRD pattern FeNC, NiNC and FeNiNC catalysts.

#### Electrochemical characterization

The electrocatalytic performance of the prepared catalysts towards ORR and OER was investigated through LSV. Prior to this, CVs were conducted in  $N_2$ - and  $O_2$ - saturated 0.1 M KOH solution to activate the electrode with a potential (E) range from -0.1 to 1.6 V vs RHE (Figure 3). Enhanced current density in the OER region is observed for FeNiNC, regardless the type of the gas saturating the electrolyte. In contrast, in the ORR region, no peaks were detected in  $N_2$ -saturated 0.1 M KOH for FeNC, NiNC and FeNiNC (broken lines in Figure 3). When the electrolyte was saturated with oxygen, a well-defined reduction peak can be seen for all samples demonstrating the occurrence of ORR at the surface of the catalysts.

To investigate the bifunctional performance of the catalysts, LSV measurements were recorded in O<sub>2</sub>- saturated 0.1 M KOH solution with a potential range first from 1.2 to 0.2 V vs RHE for ORR and then from 1.2 to 1.76 V vs RHE for OER (Figure 4a). The overall oxygen electrode activity is commonly evaluated via the difference voltage gap ( $\Delta E$ ) between the potential at current density of 10 mA cm<sup>-2</sup> ( $E_{\rm J10}$ ) for OER and the theoretical halfwave potential ( $E_{\rm I/2}$ ) for ORR from the bifunctional polarization curves of the as-prepared catalysts [47,48].

Journal Name ARTICLE

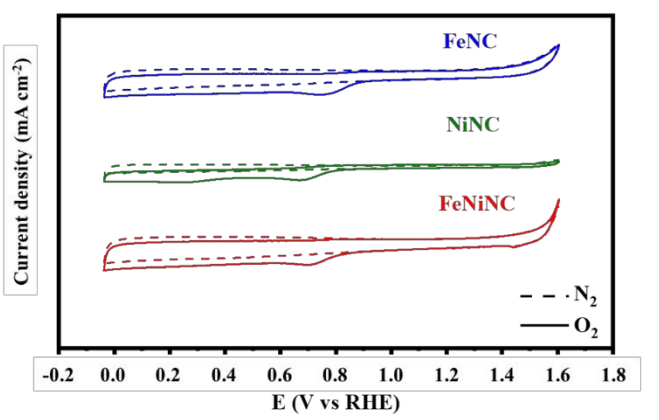


Figure 3. CV of FeNC, NiNC and FeNiNC catalysts at 10 mV s<sup>-1</sup> scan rate.

According to this approach, the polarization curves in Figure 4a indicate the FeNiNC catalyst to own the best bi-functional activity. The result in FeNiNC exhibiting a  $\Delta E$  value of 0.76 V is much lower than those of FeNC (0.85 V) and NiNC (0.89 V) (Figure 4a). Figure 4b shows the ORR activity of all catalysts, evidencing the half-potential for FeNiNC (0.81 V) to be only intermediate between FeNC (0.86 V) than and NiNC (0.77 V). The Tafel plots of the catalysts towards ORR, realized plotting the half-wave potential values versus the logarithm of the current density, are reported in Figure 4c. Their linear fit shows the lowest slope, i.e., the fastest reaction kinetics, for FeNC (65 mV dec $^{-1}$ ) followed by FeNiNC and NiNC (respectively, 68 and 74 mV dec $^{-1}$ ).

Figure 4d shows the OER activity of FeNiNC (1.57 V) electrocatalyst to be substantially better than those of FeNC, (1.75 V) and NiNC (1.66 V). Concerning the OER activity, the overpotential ( $\eta$ ) at 10 mA cm<sup>-2</sup> of FeNiNC is 340 mV (Figure 4d), i.e., much lower than those of NiNC ( $\eta$  = 430 mV) and FeNC ( $\eta$  = 520 mV), indicating that the iron-nickel alloy plays a vital role as the catalytic active site for the oxygen evolution reaction. The incorporation of Fe into Ni alters the 3d orbital band structure of the latter, enlarging metal-O covalency, which promotes electron transfer between metal cation and O adsorbates. This facilitates the extraction of electrons from oxygen, thereby accelerating the OER process [48]. In Figure 4e, the Tafel slope of FeNiNC is 47 mV dec<sup>-1</sup>, being smaller than that of NiNC (55 mV dec<sup>-1</sup>) and FeNC (64 mV dec<sup>-1</sup>), indicating fast kinetics for the OER reaction of FeNiNC.

The obtained  $\Delta E$  values are compared in Table 1 with those previously reported in the literature, showing FeNiNC has a bifunctional OER/ORR activity comparable or even better than that of other Fe and Ni based catalysts. The dual-metal active sites of Fe and Ni promote efficient adsorption and activation of oxygen intermediates during the OER, although they slightly weaken oxygen binding during the ORR, resulting in a minor decrease in  $E_1/2$  for FeNiNC. In SWBs, both OER and ORR are critical due to their sluggish kinetics [54,55], and the OER competes with the chlorine evolution reaction (CER), making OER selectivity essential for safe and efficient operation. Therefore, catalysts for SWBs are expected to exhibit well-balanced OER and ORR activities. Accordingly, SWBs were

assembled (see Figure 5) using FeNiNC with the lowest AE and compared with the benchmark Pt/C-RuOP for Peference F00907C

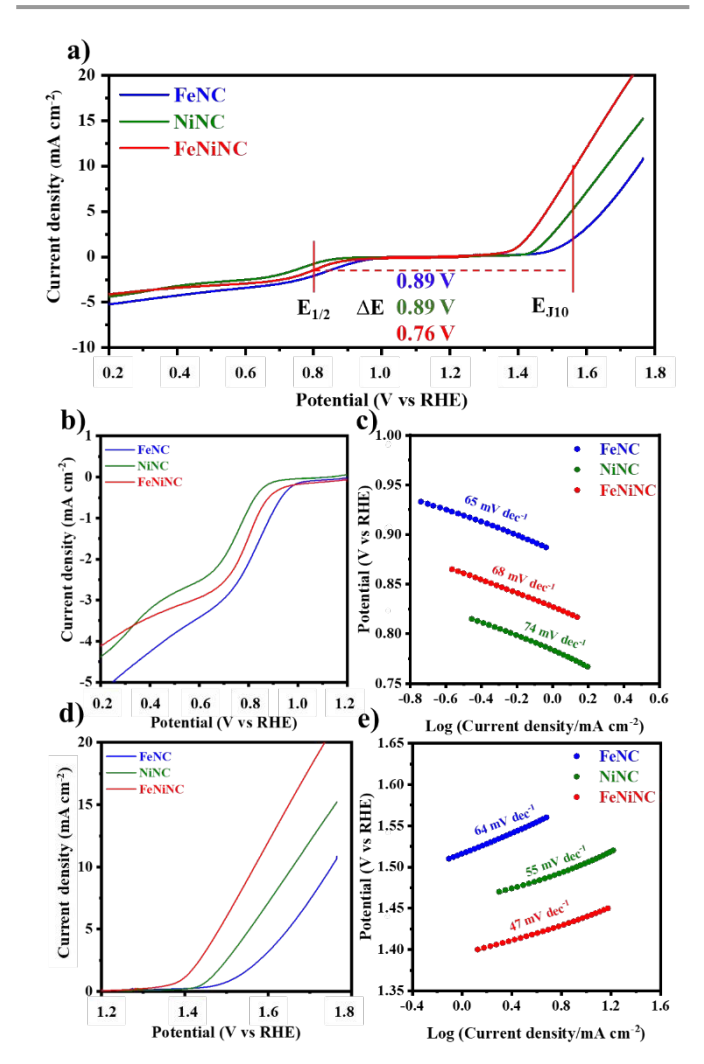


Figure 4. LSV with RDE at a scan rate of 10 mV  $s^{-1}$  and rotation speed of 1600 rpm in O<sub>2</sub>-staurated (0.1 M) KOH electrolyte: (a) overall LSV polarization curve (b) LSV curve for ORR and (c) corresponding Tafel plots, (d) LSV curves for OER and (e) corresponding Tafel plot of FeNC (blue), NiNC (green) and FeNiNC catalysts (red).

Table 1. Comparison of the bifunctional performance of FeNiNC electrocatalysts.

	000	050	•= () ()	2.6
Catalysts	ORR	OER	ΔE (V)	Refs.
	E <sub>1/2</sub>	E <sub>J10</sub>		
	(V vs RHE)	(V vs RHE)		
FeNiSAs/NC	0.88	1.64	0.76	49
Fe-NiNC-50	0.88	1.62	0.73	50
FeNi-NC	0.85	1.59	0.74	51
FeNi@C/NG	0.84	1.66	0.82	52
FeNi/NS-C	0.83	1.58	0.75	53
FeNiNC	0.81	1.57	0.76	This work
FeNC	0.86	1.75	0.89	This work
NiNC	0.77	1.66	0.89	This work

ARTICLE Journal Name

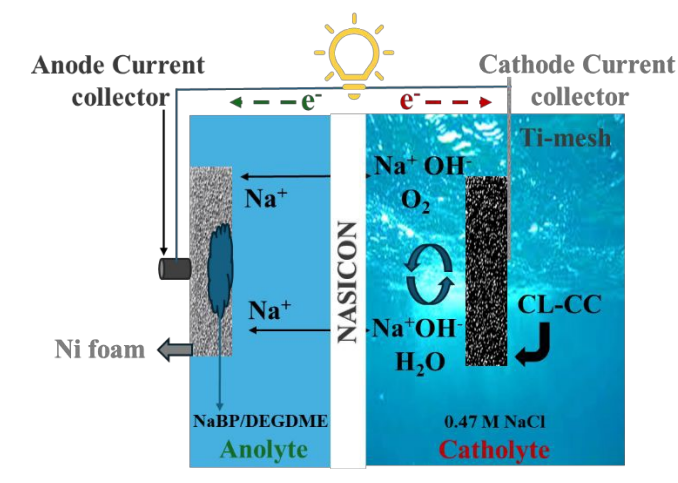


Figure 5. Schematic illustration of the cell setup for seawater-battery employing the NaBP/DEGDME solution as anolyte and 0.47 M of NaCl as catholyte. CL-CC is catalyst-loaded carbon cloth.

#### Performance of seawater batteries

The charge-discharge voltage profiles for the cell galvanostatic cycled at a current density of 0.3 mA cm<sup>-2</sup> are presented in Figure 6a. The cells were charged either up to 2 mAh or 4.0 V and discharged down to 2.5 V. The solid line represents the 1st cycle, while the dashed line corresponds to the last recorded cycle. The same analysis was performed using bare carbon cloth (CC) as the cathode. As shown in Figure S4, the SWB with bare CC exhibits a significantly higher overpotential compared to cells employing electrocatalystmodified CC, confirming the critical role of the catalyst in enhancing cell efficiency. In both Figure 6a and S4, during the first charge, Na<sup>+</sup> ions transfer from seawater to the anolyte through the NASICON separator and, finally, plating on the Ni foam current collector. From the 2<sup>nd</sup> cycle onward, the voltage profile changes since Na-BP undergoes de-sodiation during discharge. Therefore, sodiation of BP becomes evident as an additional voltage plateau at 3.15 V, in addition to the plateau due to Na plating observed at 3.4 V.

Upon the initial discharge, corresponding to Na stripping and Na-BP desodiation, the FeNiNC-based cell delivers a capacity of 2.0 mAh with a final discharge potential of 2.8 V. Although full discharge was obtained in the first five cycles, the discharge capacity became irregular in the later cycles. This instability could result from catalyst corrosion induced by Clions and/or issues in the experimental setup, such as water circulation or fluctuations in dissolved oxygen content. However, in any case, SWB cycling was feasible throughout 39 cycles, and the FeNiNC-based seawater battery retains 90.7% of its initial capacity, accompanied by a gradual decrease in discharge voltage from 2.8 V to 2.5 V. In contrast, the Pt/C-RuO<sub>2</sub> cell delivers a capacity of 1.75 mAh due to the 2.5 V cut-off (Figure 6a). During cycling, the discharge capacity increases (Figure 6b); however, it never reaches 2.0 mAh because of the higher overpotential. In the same figure, the discharge energy output of the SWBs is also presented. During cycles 10-20, the SWBs with FeNiNC show a slightly lower discharge capacity than those with Pt/C-RuO<sub>2</sub>; however, the energy output is comparable, indicating the low overpotential of the SMBs with FeNiNC.

DOI: 10.1039/D5SE00907C

Figure 6c shows the time—voltage profiles of the SWBs cell that featured FeNiNC and Pt/C-RuO<sub>2</sub> as the electrocatalyst; the former cell shows overpotential increase during the first cycles to acquire the same profile as the Pt/C-RuO<sub>2</sub>. In the case of the cell with FeNiNC, stable cycling was possible until 50 cycles (equivalent to 350 h), indicating a good performance stability.

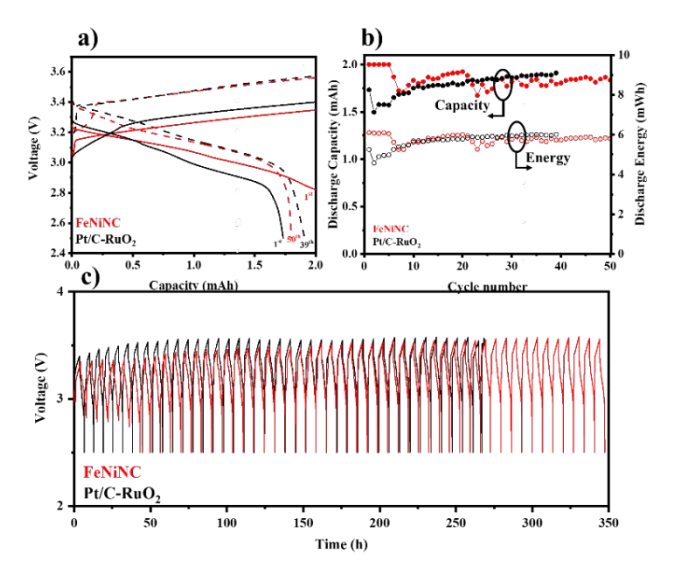


Figure 6. Galvanostatic charge-discharge of SWBs using both Pt/C-RuO $_2$  and FeNiNC as electrocatalysts at  $0.3~\rm mAcm^{-2}$ , up to 2mAh: (a) voltage profiles at 1st and 38th cycle, (b) discharge specific capacity with the discharge energy and (c) long time cycling.

#### Conclusions

A bifunctional catalyst, composed of FeNi alloys on a functionalized carbon support, prepared from urea and a biochar derived from hazelnut shells, exhibited excellent ORR-OER activity. A low differential potential of 0.76 V, between the theoretical half-potential for the ORR and the potential where current density is equal to 10 mA cm<sup>-2</sup> for the OER, was achieved. The FeNiNC electrocatalyst was successfully integrated into the cathode of seawater batteries, with a Na-BP/DEGDME anolyte, yielding promising results. Notably, the proposed catalyst material allowed enhanced long-term stability and durability of the seawater battery, compared to a commercial PGM catalyst, maintaining performance for over 350 hours at 0.3 mA cm<sup>-2</sup>.

## **Author contributions**

Conceptualization, M.A.N. and S.P.; methodology, P.P.M.P., J.M. and M.A.N.; validation, A.T. and M.A.N.; formal analysis, P.P.M.P., A.T., and J.M.; investigation, P.P.M.P., A.K., J.M. and M.A.N.; resources, M.A.N.; data curation, P.P.M.P. and A.K..; writing—original draft preparation, P.P.M.P. and J.M.; writing—review and editing, A.T., S.P., and M.A.N.; supervision, M.A.N.; project administration, M.A.N.; funding acquisition, M.A.N. All

2025. Downloaded on 23/11/25 21:19:17.

**Journal Name ARTICLE** 

authors have read and agreed to the published version of the manuscript.

# **Conflicts of interest**

The authors declare no conflicts of interest.

# **Data availability**

The data supporting this article have been included as part of the Supplementary Information.

# **Acknowledgements**

This work was developed in the framework of the project SBAM (Stoccaggio di energia con Batterie ad Acqua di Mare), CUP B87H21012170003, funded by MiTE-CSEA within the PTR (Piano Triennale di Realizzazione) 2019-2021 of the national RSE (Ricerca di Sistema Elettrico). A.T. acknowledges a financial support from the Sapienza University of Rome for the project "Catalysts for multifunctional SeaWater Batteries (C4SWB)" in the framework of ATENEO 2023 Progetti Medi (no. RM123188F7C37868).

# References

- Kim, Y.; Lee, W.-G. Green Energy and Technology Seawater Batteries Principles, Materials and Technology;
- Hwang, S.M.; Park, J.S.; Kim, Y.; Go, W.; Han, J.; Kim, Y.; Kim, Y. Rechargeable Seawater Batteries—From Concept to Applications. Advanced Materials 2019, 31.
- Abirami, M.; Hwang, S.M.; Yang, J.; Senthilkumar, S.T.; Kim, J.; Go, W.S.; Senthilkumar, B.; Song, H.K.; Kim, Y. A Metal-Organic Framework Derived Porous Cobalt Manganese Oxide Bifunctional Electrocatalyst for Hybrid Na-Air/Seawater Batteries. ACS Appl Mater Interfaces 2016, 8, 32778-32787, doi:10.1021/acsami.6b10082.
- Go, W.; Kim, J.; Pyo, J.; Wolfenstine, J.B.; Kim, Y. Investigation on the Structure and Properties of Na $_{3.1}Zr_{1.55}Si_{2.3}P_{0.7}O_{11}as$  a Solid Electrolyte and Its Application in a Seawater Battery. ACS Interfaces Appl Mater 2021, 13, 52727-52735, doi:10.1021/acsami.1c17338
- Freitas, W. da S.; Pico, P.P.M.; D'epifanio, A.; Mecheri, B. Nanostructured Fe-N-C as Bifunctional Catalysts for Oxygen Reduction and Hydrogen Evolution. Catalysts 2021, 11, doi:10.3390/catal11121525.
- Bredar, A.R.C.; Blanchet, M.D.; Burton, A.R.; Matthews, B.E.; Spurgeon, S.R.; Comes, R.B.; Farnum, B.H. Oxygen Reduction Electrocatalysis with Epitaxially Grown Spinel MnFe<sub>2</sub>O<sub>4</sub> and  $Fe_3O_4$ . ACS Catal 2022, 12, 3577-3588, doi:10.1021/acscatal.1c05172.
- Macchi, S.; Denmark, I.; Le, T.; Forson, M.; Bashiru, M.; Jalihal, A.; Siraj, N. Recent Advancements in the Synthesis and Application of Carbon-Based Catalysts in the ORR. Electrochem 2022, 3, 1-27.
- Meng, R., Zhang, C., Lu, Z., Xie, X., Liu, Y., Tang, Q., Li, H., Kong, D., Geng, C. N., Jiao, Y., Fan, Z., He, Q., Guo, Y., Ling, G., & Yang, Q. H. (2021). An Oxygenophilic Atomic Dispersed Fe-N-C Catalyst for Lean-Oxygen Seawater Batteries. Advanced Materials, 11(23). Eneray https://doi.org/10.1002/aenm.202100683

- 9 Zhao, J.-W.; Li, Y.; Luan, D.; Xiong, W.; Lou, D. Structural Evolution and Catalytic Mechanisms of Repoyskite Dxides in Electrocatalysis; 2024; Vol. 10;.
- 10 Wang, H.F.; Chen, L.; Pang, H.; Kaskel, S.; Xu, Q. MOF-Derived Electrocatalysts for Oxygen Reduction, Oxygen Evolution and Hydrogen Evolution Reactions. Chem Soc Rev 2020, 49, 1414–
- 11 Zhao, Y.; Adiyeri Saseendran, D.P.; Huang, C.; Triana, C.A.; Marks, W.R.; Chen, H.; Zhao, H.; Patzke, G.R. Oxygen Evolution/Reduction Reaction Catalysts: From In Situ Monitoring and Reaction Mechanisms to Rational Design. 2023, Rev 123, 6257-6358, doi:10.1021/acs.chemrev.2c00515.
- 12 Wang, M.; Wang, Y.; Mao, S.S.; Shen, S. Transition-Metal Alloy Electrocatalysts with Active Sites Modulated by Metal-Carbide Heterophases for Efficient Oxygen Evolution. Nano Energy 2021, 88, doi:10.1016/j.nanoen.2021.106216.
- 13 Dresp, S.; Dionigi, F.; Klingenhof, M.; Merzdorf, T.; Schmies, H.; Drnec, J.; Poulain, A.; Strasser, P. Molecular Understanding of the Impact of Saline Contaminants and Alkaline PH on NiFe Layered Double Hydroxide Oxygen Evolution Catalysts. ACS Catal 2021, 11, 6800-6809, doi:10.1021/acscatal.1c00773.
- 14 Jin, S. Are Metal Chalcogenides, Nitrides, and Phosphides Oxygen Evolution Catalysts or Bifunctional Catalysts? ACS Energy Lett 2017, 2, 1937-1938.
- 15 Hu, X.; Wang, R.; Feng, W.; Xu, C.; Wei, Z. Electrocatalytic Oxygen Evolution Activities of Metal Chalcogenides and Phosphides: Fundamentals, Origins, and Future Strategies. Journal of Energy Chemistry 2023, 81, 167–191.
- 16 Artyushkova, K.; Serov, A.; Rojas-Carbonell, S.; Atanassov, P. Chemistry of Multitudinous Active Sites for Oxygen Reduction Reaction Transition Metal-Nitrogen-Carbon Electrocatalysts. Journal of Physical Chemistry C 2015, 119, 25917-25928, doi:10.1021/acs.jpcc.5b07653.
- 17 da Silva Freitas, W.; D'Epifanio, A.; Lo Vecchio, C.; Gatto, I.; Baglio, V.; Ficca, V.C.A.; Placidi, E.; Mecheri, B. Tailoring MOF Structure via Iron Decoration to Enhance ORR in Alkaline Polymer Electrolyte Membrane Fuel Cells. Chemical Engineering Journal 2023, doi:10.1016/j.cej.2023.142987.
- 18 Aysla Costa De Oliveira, M.; D'Epifanio, A.; Ohnuki, H.; Mecheri, B. Platinum Group Metal-Free Catalysts for Oxygen Reduction Reaction: Applications in Microbial Fuel Cells. Catalysts 2020, 10.
- 19 de Oliveira, M.A.C.; Ficca, V.C.A.; Gokhale, R.; Santoro, C.; Mecheri, B.; D'Epifanio, A.; Licoccia, S.; Atanassov, P. Iron(II) Phthalocyanine (FePc) over Carbon Support for Oxygen Reduction Reaction Electrocatalysts Operating in Alkaline Electrolyte. Journal of Solid State Electrochemistry 2021, 25, 93-104, doi:10.1007/s10008-020-04537-x.
- 20 Zhang, S.; Zhang, H.; Hua, X.; Chen, S. Tailoring Molecular Architectures of Fe Phthalocyanine on Nanocarbon Supports for High Oxygen Reduction Performance. J Mater Chem A Mater 2015, 3, 10013–10019, doi:10.1039/c5ta01400j.
- 21 Taniguchi, T.; Tateishi, H.; Miyamoto, S.; Hatakeyama, K.; Ogata, C.; Funatsu, A.; Hayami, S.; Makinose, Y.; Matsushita, N.; Koinuma, M.; et al. A Self-Assembly Route to an Iron Phthalocyanine/Reduced Graphene Oxide Electrocatalyst Affording an Ultrafast Oxygen Reduction Reaction. Particle and Particle Systems Characterization 2013, 30, 1063-1070, doi:10.1002/ppsc.201300177.
- 22 Osmieri, L.; Monteverde Videla, A.H.A.; Ocón, P.; Specchia, S. Kinetics of Oxygen Electroreduction on Me-N-C (Me = Fe, Co, Cu) Catalysts in Acidic Medium: Insights on the Effect of the Transition Metal. Journal of Physical Chemistry C 2017, 121, 17796-17817, doi:10.1021/acs.jpcc.7b02455.
- 23 Chen, C.; Sun, M.; Zhang, F.; Li, H.; Sun, M.; Fang, P.; Song, T.; Chen, W.; Dong, J.; Rosen, B.; et al. Adjacent Fe Site Boosts

This article is licensed under a Creative Commons Attribution-NonCommercial 3.0 Unported Licence

2025. Downloaded on 23/11/25 21:19:17.

Open Access Article. Published on 28

**ARTICLE Journal Name** 

- Electrocatalytic Oxygen Evolution at Co Site in Single-Atom-Catalyst through a Dual-Metal-Site Design. Energy Environ Sci 2023, 16, 1685-1696, doi:10.1039/d2ee03930c.
- 24 Streb, C., Chen, Z., Cheng, W., Cao, K., Meng, J., Rahali, S., Ebrahimi, E., Chala, S. A., Ma, N., Liu, R., Lakshmanan, K., Cheung, C.-C., Chang, C.-Y., Luo, H., Wang, Y., & Hwang, B. J. (2024). A Bifunctional Iron-Nickel Oxygen Reduction / Oxygen Evolution Catalyst for High-Performance Rechargeable Zinc-Batteries. https://doi.org/10.26434/chemrxiv-2024-<u>d4</u>885
- 25 Zhu, X., Zhang, D., Chen, C. J., Zhang, Q., Liu, R. S., Xia, Z., Dai, L., Amal, R., & Lu, X. (2020). Harnessing the interplay of Fe-Ni atom pairs embedded in nitrogen-doped carbon for bifunctional oxygen electrocatalysis. Nano Energy, 71. https://doi.org/10.1016/j.nanoen.2020.104597
- 26 Wu, X., Yang, Z., Li, C., Shao, S., Qin, G., & Meng, X. (2025). Organizational and Mechanistic Modulation of ORR/OER Activity in M1M2-N-C Bimetallic Catalysts. ACS Catalysis, 15(1), 432–446. https://doi.org/10.1021/acscatal.4c06280
- 27 Gao, W.; Lin, Z.; Chen, H.; Yan, S.; Huang, Y.; Hu, X.; Zhang, S. A Review on N-Doped Biochar for Enhanced Water Treatment and Emerging Applications. Fuel Processing Technology 2022,
  - doi:https://doi.org/10.1016/j.fuproc.2022.107468.
- 28 Hou, G.; Wu, J.; Li, T.; Lin, J.; Wang, B.; Peng, L.; Yan, T.; Hao, L.; Qiao, L.; Wu, X. Nitrogen-Rich Biomass Derived Three-Dimensional Porous Structure Captures FeNi Metal Nanospheres: An Effective Electrocatalyst for Oxygen Evolution Reaction. Int J Hydrogen Energy 2022, 47, 12487-12499, doi:10.1016/j.ijhydene.2022.02.004.
- 29 Kim, Y.; Kim, J.K.; Vaalma, C.; Bae, G.H.; Kim, G.T.; Passerini, S.; Kim, Y. Optimized Hard Carbon Derived from Starch for Rechargeable Seawater Batteries. Carbon N Y 2018, 129, 564-571, doi:10.1016/j.carbon.2017.12.059.
- 30 Susanto, S.; Nurtono, T.; Widiyastuti, W.; Yeh, M.H.; Setyawan, H. Controlling N-Doping Nature at Carbon Aerogels from Biomass for Enhanced Oxygen Reduction in Seawater ACS 2024, 13994-14004. Batteries. Omega 9, doi:10.1021/acsomega.3c09297.
- 31 Wang, B.; Wang, Y.; Peng, Y.; Wang, X.; Wang, N.; Wang, J.; Zhao, J. Nitrogen-Doped Biomass-Based Hierarchical Porous Carbon with Large Mesoporous Volume for Application in Energy Storage. Chemical Engineering Journal 2018, 348, 850-859, doi:https://doi.org/10.1016/j.cej.2018.05.061.
- 32 Beda, A.; Le Meins, J.-M.; Taberna, P.-L.; Simon, P.; Matei Ghimbeu, C. Impact of Biomass Inorganic Impurities on Hard Carbon Properties and Performance in Na-Ion Batteries. Sustainable Materials and Technologies 2020, 26, e00227, doi:https://doi.org/10.1016/j.susmat.2020.e00227.
- 33 Liu, X.; Yang, X.; Zhao, Z.; Fang, T.; Yi, K.; Chen, L.; Liu, S.; Wang, R.; Jia, X. Isolated Binary Fe-Ni Metal-Nitrogen Sites Anchored on Porous Carbon Nanosheets for Efficient Oxygen Electrocatalysis through High-Temperature Gas-Migration Strategy. ACS Appl Mater Interfaces 2024, 16, 18703–18712, doi:10.1021/acsami.3c17193.
- 34 Snitkoff-Sol, R. Z., Presman, Y., & Elbaz, L. (2025). Investigating the Fuel Cell Performance Tradeoffs of Thick Catalyst Layers. ChemElectroChem, 12(10), https://doi.org/10.1002/celc.202500038.
- 35 Luo, J., Yi, Y., & Fang, Z. (2023). Nitrogen-rich magnetic biochar prepared by urea was used as an efficient catalyst to activate persulfate to degrade organic pollutants. Chemosphere, https://doi.org/10.1016/j.chemosphere.2023.139614
- 36 Zhao, C., Ge, L., Li, X., Zuo, M., Xu, C., Chen, S., Li, Q., Wang, Y., & Xu, C. (2023). Effects of the carbonization temperature and intermediate cooling mode on the properties of coal-

- Energy, 273. based activated carbon. https://doi.org/10.1016/j.energy.2023<sub>D</sub>137177039/D5SE00907C
- 37 Li, H., Kang, W., Wang, L., Yue, Q., Xu, S., Wang, H., & Liu, J. (2013). Synthesis of three-dimensional flowerlike nitrogendoped carbons by a copyrolysis route and the effect of nitrogen species on the electrocatalytic activity in oxygen reduction reaction. Carbon, 54, https://doi.org/10.1016/j.carbon.2012.11.036
- 38 Barszcz, W., Łożyńska, M., & Molenda, J. (2024). Impact of pyrolysis process conditions on the structure of biochar obtained from apple waste. Scientific Reports, 14(1). https://doi.org/10.1038/s41598-024-61394-8
- 39 Ma, D., Zhang, Y., Liang, M., Niu, R., Ge, Y., Zou, Y., & Dong, X. (2025). Effect of the Microstructure of Carbon Supports on the Oxygen Reduction Properties of the Loaded Non-Noble Metal Catalysts. Nanomaterials, 15(17). https://doi.org/10.3390/nano15171327
- 40 Chen, W., Chen, Y., Yang, H., Li, K., Chen, X., & Chen, H. (2018). Investigation on biomass nitrogen-enriched pyrolysis: Influence of temperature. Bioresource Technology, 249, 247-253. https://doi.org/10.1016/j.biortech.2017.10.022
- 41 Clair, B., Ruelle, J., & Beauchene, J. (2009). Mesoporosity as a new parameter for understanding tension stress generation in trees. Article in Journal of Experimental Botany. https://doi.org/10.1093/jxp/erp133.
- 42 Yuan, D. S., Zhou, T. X., Zhou, S. L., Zou, W. J., Mo, S. S., & Xia, N. N. (2011). Nitrogen-enriched carbon nanowires from the direct carbonization of polyaniline nanowires and its Electrochemistry properties. electrochemical Communications, 13(3), 242-246. https://doi.org/10.1016/j.elecom.2010.12.023
- 43 Ren, S., Tang, X., Zhang, P., Peng, W., Zeng, X., Zheng, H., & Wan, Z. (2025). Multi-scale porous nitrogen-rich large carbon networks modified by bimetallic FeNi alloys as exceptional bifunctional catalysts for rechargeable Zn-air batteries. Energy Journal of Storage, https://doi.org/10.1016/j.est.2024.114740.
- 44 Deng, S.; Han, X.; Lv, N.; Yang, X.; Liu, Q.; Jiang, Y.; Yang, Y.; Xi, B. Unveiling the Activation Mechanism: The Role of Nitrogen-Doped Biochar in Enhancing Fe(VI) Catalysis. Chemical Engineering Journal doi:10.1016/j.cej.2024.150263.
- 45 Wang, Y., Nong, W., Gong, N., Salim, T., Luo, M., Tan, T. L., Hippalgaonkar, K., Liu, Z., & Huang, Y. (2022). Tuning Electronic Structure and Composition of FeNi Nanoalloys for Enhanced Oxygen Evolution Electrocatalysis via a General Synthesis Strategy. Small. https://doi.org/10.1002/smll.202203340
- 46 el Boraei, N. F., Ibrahim, M. A. M., & Naghmash, M. A. (2022). Nanocrystalline FeNi alloy powder prepared by electrolytic synthesis; characterization and its high efficiency in removing Remazol Red dye from aqueous solution. Journal of Physics Solids, Chemistry of https://doi.org/10.1016/j.jpcs.2022.110714
- 47 Chen, Z., Zeng, J., Dong, X., Liu, Z., Wang, J., & Zhong, Q. (2025). The enhanced fast-charging and cycle stability for high energy efficiency KI-assisted rechargeable zinc-air batteries. Journal of Power Sources, https://doi.org/10.1016/j.jpowsour.2025.237286.
- 48 Wu, X., Tang, C., Cheng, Y., Min, X., Jiang, S. P., & Wang, S. (2020). Bifunctional Catalysts for Reversible Oxygen Evolution Reaction and Oxygen Reduction Reaction. In Chemistry - A European Journal (Vol. 26, Issue 18, pp. 3906-3929). John Wiley and Sons https://doi.org/10.1002/chem.201905346
- 49 Gopalakrishnan, M., Kao-lan, W., Rittiruam, M., Praserthdam, S., Praserthdam, P., Limphirat, W., Nguyen, M. T., Yonezawa, T., & Kheawhom, S. (2024). 3D Hierarchical MOF-Derived

View Article Online

**Journal Name ARTICLE** 

Defect-Rich NiFe Spinel Ferrite as a Highly Efficient Electrocatalyst for Oxygen Redox Reactions in Zinc-Air DOI: 10.1039/D5SE00907C Batteries. ACS Applied Materials and Interfaces, 16(9), 11537-11551. https://doi.org/10.1021/acsami.3c17789.

- 50 Zhu, X.; Zhang, D.; Chen, C.-J.; Zhang, Q.; Liu, R.-S.; Xia, Z.; Dai, L.; Amal, R.; Lu, X. Harnessing the Interplay of Fe-Ni Atom Pairs Embedded in Nitrogen-Doped Carbon for Bifunctional Oxygen Electrocatalysis. Nano Energy 2020, 71, 104597, doi:https://doi.org/10.1016/j.nanoen.2020.104597.
- 51 Liu, C.; Wu, S.; Tian, S.; Yang, J.; Li, J.; Guan, Q.; Yin, F.; Xiang, X.; Wang, Y.; Meng, X.; et al. Structurally Optimized Rosettelike Microspheres Carbon with Fe-Ni Single Atom Sites for Bifunctional Oxygen Electrocatalysis in Zinc-Air Batteries. Chemical Engineering Journal 2024, 497, 154963, https://doi.org/10.1016/j.cej.2024.154963.
- 52 Li, G.L.; Yang, B.B.; Xu, X.C.; Cao, S.; Shi, Y.; Yan, Y.; Song, X.; Hao, C. FeNi Alloy Nanoparticles Encapsulated in Carbon Shells Supported on N-Doped Graphene-Like Carbon as Efficient and Stable Bifunctional Oxygen Electrocatalysts. Chemistry - A European Journal 2020, 26, 2890-2896, doi:10.1002/chem.201904685.
- 53 ai, J.; Hao, X.; Bian, Z.; Wu, Y.; Wei, C.; Yin, X.; Liu, B.; Fang, M.; Lv, Y.; Xie, Y.; et al. Elucidating the Discrepancy between the Intrinsic Structural Instability and the Apparent Catalytic Steadiness of M-N-C Catalysts toward Oxygen Evolution Reaction. Angewandte Chemie - International Edition 2024, 63, doi:10.1002/anie.202409079.
- 54 Huang, T., Guo, M., Li, W., Bao, Y., Yu, A., Li, D. S., Tu, J., Wang, M., Hao, W., & Sun, C. (2024). High-performance oxygen evolution reaction via self-optimizing interface engineering with simultaneous activation of dual-sites of surface oxyhydroxides. Applied Surface Science, https://doi.org/10.1016/j.apsusc.2024.159936
- 55 Wu, J., Chong, R., Li, Z., Xu, S., Liu, Y., He, X., Qian, J., Zhang, J., Wang, L., & Zhang, Z. H. (2025). Tailoring Active Sites in Amorphous NiFe-MOFs through Pyridine Ligand Coordination for Enhanced Oxygen Evolution Performance. ACS Applied Interfaces, 52297-52306. Materials *17*(37), https://doi.org/10.1021/acsami.5c14277
- 56 Arnold, S., Wang, L., & Dual-Use of Search Seawater Batteries for Energy Storage and Water Desalination. In Small (Vol. 18, Issue 43). John Wiley and Sons Inc. https://doi.org/10.1002/smll.202107913

View Article Online DOI: 10.1039/D5SE00907C

# **Data Availability Statement**

• The data supporting this article have been included as part of the Supplementary Information.